A Priori Evaluation of Aqueous Polarization Effects Through Monte Carlo QM-MM Simulations

Jiali Gao* and Xinfu Xia

A Monte Carlo quantum mechanical–molecular mechanical (QM-MM) simulation method was used to determine the contributions of the solvent polarization effect to the total interaction energies between solute and solvent for amino acid side chains and nucleotide bases in aqueous solution. In the present AM1-TIP3P approach, the solute molecule is characterized by valence electrons and nucleus cores with Hartree-Fock theory incorporating explicit solvent effects into the total Hamiltonian, while the solvent is approximated by the three–point charge TIP3P model. The polarization energy contributes 10 to 20 percent of the total electrostatic energy in these systems. The performance of the hybrid AM1-TIP3P model was further validated by consideration of bimolecular complexes with water and by computation of the free energies of solvation of organic molecules using statistical perturbation theory. Excellent agreement with ab initio 6-31G(d) results and experimental solvation free energies was obtained.

A great challenge in statistical mechanical Monte Carlo and molecular dynamics simulations of chemical reactions in solution is to incorporate explicitly the solvent polarization effects into the potential surface (*1*, *2*). However, because of the complexity in computational details, two-body potential functions are widely used in protein and fluid simulations (*3*, *4*). A key feature in these effective pairwise potential functions is that the many-body polarization effects are incorporated in an average way into the parameters fitted to reproduce experimental fluid properties (*5*, *6*). As a result, the charge distribution designed for liquid simulations normally leads to dipole moments that are about 10 to 20% greater than gas-phase values (*5*, *6*). Undoubtedly, a knowledge of the quantitative polarization effects in solution is of great interest and significance. Two questions are directly relevant: (i) Can condensed-phase polarization effects be systematically evaluated a priori in fluid simulations? and (ii) What is the quantitative contribution of polarization energy to the total electrostatic interaction between the solute and solvent? In this report, we use a combined quantum mechanical (QM) and molecular mechanical (MM) approach, developed by many researchers (*7–11*), in Monte Carlo simulations (*12*) and demonstrate how this hybrid QM-MM method can be used in the systematic computation of the polarization energies through Hartree-Fock molecular orbital (MO) theory incorporating explicit solvent effects in statistical mechanical Monte Carlo simulations. The quantitative insights from this energy decomposition method would increase our understanding of molecular interactions and chemical processes in solution and in the enzymatic environment.

In the hybrid QM-MM approach, part of the system, for example, the solute molecule or the active site region of an enzyme, is treated quantum mechanically, whereas the "environmental" solvent molecules are approximated by molecular mechanical potentials (*7–12*). The idea can be traced back to Bernal and Fowler, who proposed the partitioning of a condensed-phase system into discrete solute and continuum solvent regions (*13*), and has been extensively exploited in recent years, particularly in energy minimization studies of enzymatic reaction paths (*7–12*, *14*). However, there have been only few applications of the hybrid QM-MM model in fluid simulations because of the limitation of computer speed (*12*, *15*).

For the QM region, the closed-shell restricted Hartree-Fock wave function Φ is written as a single Slater determinant of N doubly occupied molecular orbitals, $\{\psi_i\}$:

$$\Phi = |\psi_1\alpha(1)\psi_1\beta(2)\cdots\psi_N\beta(2N)> \quad (1)$$

where α and β are the electron spin eigenfunctions and the MOs are linear combinations of atomic basis sets, $\{\phi_\mu\}$. The total effective Hamiltonian of the system is as follows (*7*, *12*):

$$\hat{H}_{\text{eff}} = \hat{H}^0 + \hat{H}_{\text{QM/MM}} + \hat{H}_{\text{MM}} \quad (2)$$

where $\hat{H}^0$ is the Hamiltonian for the isolated QM molecule, $\hat{H}_{\text{MM}}$ is the solvent interaction energy determined by empirical potentials, and $\hat{H}_{\text{QM/MM}}$ is the solute-solvent interaction Hamiltonian defined by Eq. 3:

$$\hat{H}_{\text{QM/MM}} = \hat{H}^{\text{el}}_{\text{QM/MM}} + E_{\text{vdW}} = -\sum_{s=1}^{S}\sum_{i=1}^{2N}\frac{eq_s}{R_{si}} + \sum_{s=1}^{S}\sum_{m=1}^{M}\frac{q_sZ_m}{R_{sm}} + \sum_{s=1}^{S}\sum_{m=1}^{M}4\epsilon_{sm}\left[\left(\frac{\sigma_{sm}}{R_{sm}}\right)^{12} - \left(\frac{\sigma_{sm}}{R_{sm}}\right)^{6}\right] \quad (3)$$

where e is the electron charge, q_s and Z_m are, respectively, charges on the solvent and solute nuclear centers, S and M are the corresponding total number of interaction sites, and R_{si} and R_{sm} are the distances of the solute electrons and nuclei from the solvent sites, respectively. The Lennard-Jones term in Eq. 3 is needed because of the hybrid interaction between the QM and MM regions; it contains the only adjustable parameters for the solute (σ_m and ϵ_m) in the present approach (*7*, *12*, *16*). The combining rules used for the solute-solvent interactions are $\sigma_{sm} = (\sigma_s\sigma_m)^{1/2}$ and $\epsilon_{sm} = (\epsilon_s\epsilon_m)^{1/2}$.

The total interaction energy between a QM solute and an MM solvent, E_{sx}, consists of contributions from the van der Waals (vdW) and electrostatic (el) interactions (Eq. 3). The latter is given by Eq. 4 and can be written in terms of solute-solvent perturbations:

$$E^{\text{el}}_{sx} = <\Phi|\hat{H}^0 + \hat{H}^{\text{el}}_{\text{QM/MM}}|\Phi> - <\Phi^0|\hat{H}^0|\Phi^0> = E^{(1)} + E^{(2)} + \cdots \quad (4)$$

where Φ^0 and Φ, respectively, are defined by $\hat{H}^0|\Phi^0> = E^{(0)}|\Phi^0>$ and $\hat{H}_{\text{eff}}|\Phi> = E_{\text{tot}}|\Phi>$, or the wave functions in the gas phase and solution, respectively. The first-order perturbation term ($E^{(1)} = <\Phi^0|\hat{H}^{\text{el}}_{\text{QM/MM}}|\Phi^0>$) in Eq. 4 is the interaction energy between the "unpolarized" solute and the solvent, whereas all other higher order terms consist of modifications to the wave function and contribute to the solute-solvent polarization energy, which can formally be defined as $E_{\text{pol}} = E^{\text{el}}_{sx} - E^{(1)}$, or

$$E^{\text{el}}_{sx} = E^{(1)} + E_{\text{pol}} \quad (5)$$

Because Φ^0 and Φ are solved in Monte Carlo or molecular dynamics simulations, E_{pol} can exactly be computed, and there is no need to carry out perturbation calculations. Importantly, the polarization energy can further be decomposed into two terms: (i) a solute electron distortion energy, E_{dist} (Eq. 6), which yields a positive value for reorganizing (or polarizing) the solute electron distribution in solution; and (ii) a net gain in interaction energy between the polarized solute and the bulk solvent over that of an "unpolarized" solute (Eq. 7):

$$E_{\text{dist}} = <\Phi|\hat{H}^0|\Phi> - <\Phi^0|\hat{H}^0|\Phi^0> \quad (6)$$

$$\Delta E_{\text{QM/MM}} = <\Phi|\hat{H}^{\text{el}}_{\text{QM/MM}}|\Phi> - <\Phi^0|\hat{H}^{\text{el}}_{\text{QM/MM}}|\Phi^0> \quad (7)$$

Therefore,

$$E_{\text{pol}} = E_{\text{dist}} + \Delta E_{\text{QM/MM}} \quad (8)$$

Department of Chemistry, State University of New York at Buffalo, Buffalo, NY 14214.

*To whom correspondence should be addressed.

The interpretation of these terms is straightforward; $E^{(1)}$ is the interaction energy between the unperturbed solute with gas-phase electron distribution and the surrounding solvent, whereas $<\Phi|\hat{H}_{QM/MM}|\Phi>$ is the interaction energy "after" the polarization. Thus, $\Delta E_{QM/MM}$ is the net gain in solute-solvent interaction energy owing to the solute electronic polarization in aqueous solution (*17*). The energy penalty for distorting or polarizing the solute electron density to create the electron distribution in solution is given by E_{dist} and is one-half of the gain in interaction energy according to classic linear response theory (*11*, *18*). All quantities are computed through statistical mechanical Monte Carlo simulations to yield the macroscopic ensemble averages in the present study. Furthermore, electric dipole moments of the solute molecules can be obtained with standard methods in ab initio MO calculations (*19*), whereas the induced dipole moments (μ_{ind}) in aqueous solution are determined from differences between the values obtained in the gas phase and in water.

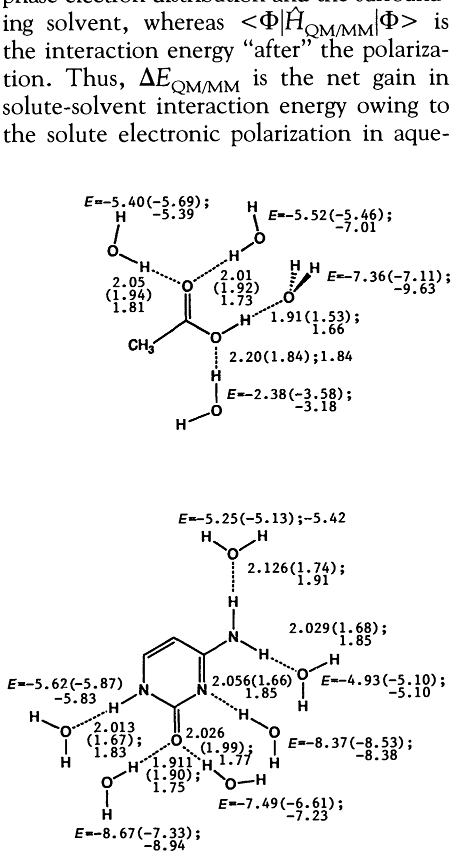

Fig. 1. Molecule-water complexes for acetic acid and cytosine: 6-31G(d) values for the interaction energies in kilocalories per mole, and distances in angstroms are followed by the AM1-TIP3P (in parentheses), and OPLS (*5*) results, respectively. Monomer geometries are fixed in the energy minimizations. Hydrogen bond distances for water acceptor complexes predicted by the AM1-TIP3P model are typically 0.15 Å shorter than the OPLS values (*5*), whereas agreement between the AM1-TIP3P and the 6-31G(d) results for donor water complexes is excellent.

We illustrate the QM-MM polarization energy decomposition method for a series of organic molecules of biological interest in aqueous solution, representing major amino acid functional groups and nucleotide bases. The Monte Carlo QM-MM simulations were performed in a cubic box consisting of 216 or 260 TIP3P (*20*) water monomers plus one solute at 25°C and 1 atm with the NPT ensemble (*21*). The semiempirical MO theory developed by Dewar and co-workers, namely, the Austin Model 1 (AM1) (*22*, *23*), was used to form the AM1-TIP3P force field. The major advantages of using a semiempirical QM method include its high computational efficiency (about 1000 times faster than ab initio calculations at comparable levels) and excellent results for many systems that have been parameterized (*7*, *22*). This approach enables the QM energy to be computed throughout the Monte Carlo simulation (*12*), which would be difficult with the use of ab initio techniques for large molecules as considered here. The latter approach, however, can systematically improve the accuracy of the QM computations (*19*).

In order to verify the performance of the AM1-TIP3P model, we investigated bimolecular complexes with water. The organic species were treated quantum mechanically (AM1) and the water was treated molecular mechanically with the TIP3P potential. Two representative systems with optimized geometries and energies are shown in Fig. 1, and the accord for the interaction energies between the AM1-TIP3P and ab initio results is illustrated in Fig. 2 for a total of 53 complexes. Overall, the agreement is excellent with a root-mean-square (rms) deviation of 0.84 kcal/mol. Large discrepancies are mainly from ion-water complexes, without which the rms deviation would be 0.62 kcal/mol, similar to the best fit between empirical potentials and ab initio calculations (*5*). Thus, the result shown in Fig. 2 provides strong support to the validity of the hybrid AM1-TIP3P model, suggesting that the simulation results, although approximate, may be used to obtain insights into the specific contributions to the polarization effects.

Energetic results for amino acid side chains are given in Table 1. The total solute-solvent interaction energy E_{sx} is de-

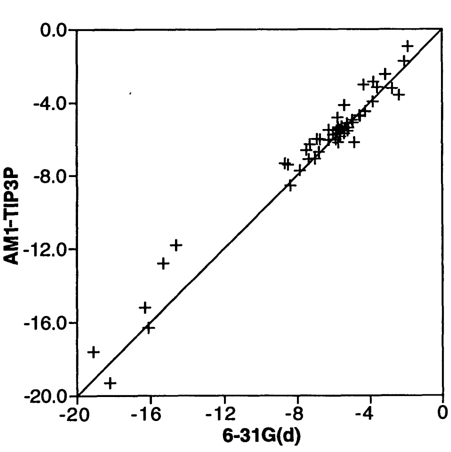

Fig. 2. Comparison between ab initio 6-31G(d) and AM1-TIP3P interaction energies.

Table 1. Computed solvation free energies (ΔG_{sol}) and solute-solvent interaction energies (kilocalories per mole). Average energies in aqueous solution were obtained in Monte Carlo simulations of one solute plus 216 water molecules, with the solute monomer treated quantum mechanically throughout. Each simulation consisted of 5 × 10^5 to 10^6 configurations for equilibration, followed by averaging for 1.5 × 10^6 configurations. The configurations were chosen with Metropolis and preferential sampling. Free energies of solvation are relative to ethane and are computed first by electrostatic decoupling of the QM Hamiltonian followed by statistical perturbation calculations transforming the van der Waals spheres into ethane (*12*, *25*). At least four windows of double-wide sampling were used to span the whole transformation; each window consisted of 1 × 10^6 to 1.5 × 10^6 configurations for averaging. Experimental free energies are taken from (*26*) and are similar to the electrostatic free energies of Honig and co-workers (*2*). We obtained error bars (±1σ) by computing separate averages over blocks of 10^5 configurations during the simulation. They are approximately ±0.5 kcal/mol for ΔG_{sol}, ±1 kcal/mol for E_{sx}, and ±0.2 kcal/mol for E_{pol}.

Compound	$E^{(1)}$	E_{dist}	$\Delta E_{QM/MM}$	E_{pol}	E_{vdW}	E_{sx}	$\Delta\Delta G_{sol}$	$\Delta\Delta G_{sol}$ (expt)
CH_4	0.7	0.1	−0.2	−0.1	−2.3	−1.6	1.2	0.2
CH_3CH_3	1.3	0.1	−0.3	−0.1	−4.0	−2.9	0.0	0.0
C_6H_6	0.7	0.5	−0.9	−0.5	−9.3	−9.0	0.3	−2.6
H_2O	−11.5	1.3	−3.8	−2.5	−0.1	−14.0	−8.3	−8.1
CH_3OH	−9.4	1.5	−3.1	−1.6	−2.7	−13.7	−6.2	−6.9
CH_3OCH_3	−4.7	0.8	−1.6	−0.8	−4.7	−10.3	−3.6	−3.7
CH_3COCH_3	−9.6	2.0	4.0	−2.0	−6.4	−18.0	−5.0	−5.6
CH_3NH_2	−4.5	0.4	−0.8	−0.4	−3.0	−7.9	−4.0	−6.4
CH_3CN	−3.7	1.3	−2.6	−1.3	−4.7	−9.7	−3.1	−5.7
NMA	−15.6	3.8	−7.6	−3.8	−6.9	−26.4	−8.5	−12.0
syn-CH_3CO_2H	−15.5	1.8	−3.6	−1.8	−4.9	−22.1	−8.4	−8.5
anti-CH_3CO_2H	−22.4	3.8	−7.9	−4.2	−5.2	−31.8		
Imidazole	−10.5	2.3	−4.6	−2.3	−6.7	−19.5	−7.2	−6, −12.0
$CH_3CO_2^-$	−132	3.9	−7.9	−4.0	−1.7	−138	−80	−79
$CH_3NH_3^+$	−116	1.1	−2.2	−1.1	−0.4	−117		
$(CH_3)_3C^+$	−89	0.4	−0.8	−0.4	−6.1	−95		

termined by electrostatic and van der Waals contributions, of which the electrostatic interaction energy is divided into permanent $E^{(1)}$ and polarization terms (Eq. 8). Although the main objective of the present study was to determine the solute polarization energy in aqueous solution, relative free energies of hydration were computed for several species by the method developed recently with statistical perturbation theory (*12*, *24*, *25*). These calculations are very demanding of computer time because multistep simulations are required (*25*). The computed free energy changes are in good agreement with experimental values (*26*), with an error range similar to that observed in calculations in which empirical force fields were used (*25*). The agreement further demonstrates the reliability of the AM1-TIP3P model for quantitative energetic evaluations.

Several trends are apparent. In all cases, there is a substantial polarization contribution to the total electrostatic interaction energy, ranging from 10 to 20%. Of course, it is well known that molecules are polarized in polar solvent; however, quantitative contributions are not clear, particularly for protein and DNA systems in aqueous solution (*1*–*4*). Our results indicate that the polarization effect is significant and that the polarization energy can amount to about one-half of a hydrogen bond for a single peptide unit. Discussions of protein allosteric mechanism, molecular recognition, and ligand-substrate binding are often expressed in terms of hydrogen bonding (*27*). It appears necessary to also consider the environmental polarization effects for processes involving the transfer of a functional group from aqueous exposure to the hydrophobic protein core where solvent polarization is less important. Furthermore, there is clearly some correlation between the computed induced dipole moments, electric polarization energy, and solute-solvent electrostatic interaction energy (Fig. 3). The slope of Fig. 3 represents the percentage of the polarization contribution to the total electrostatic interaction. The computed numerical values in the penalty for creating the polarized electron distribution, E_{dist}, are indeed one-half of the energy gain between solute-solvent interactions (Table 1), in accord with classical macroscopic theory.

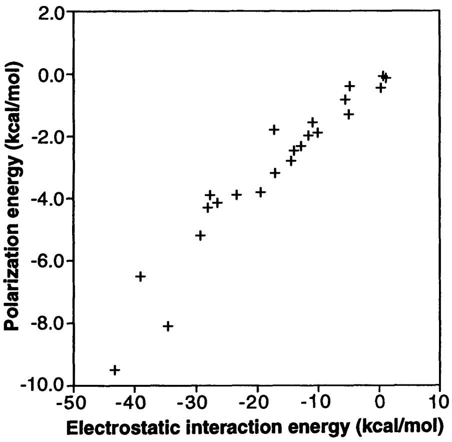

Fig. 3. Correlation between calculated solute electric polarization and total solute-solvent electrostatic interaction energies.

The calculated and experimental dipole moments are summarized in Table 2. In all cases, the AM1 method gives excellent predictions on the dipole moments for the isolated molecules in comparison with the experimental data (*22*), whereas the computed dipole moments in aqueous solution are significantly greater than the corresponding gas-phase values, resulting in large induced dipole moments for these compounds. Experimental dipole moments of simple organic molecules in water are not available, making direct comparison difficult (*28*), although the calculated results are consistent with the predictions of Cramer and Truhlar for similar compounds with self-consistent field (SCF) solvation model (*29*, *30*). A special case is the hydration of water, in which the computed dipole moment (2.15 D) may be compared with the experimental estimate for bulk water (2.3 to 2.4 D) (*1*); the accord is good. The average dipole moment $|<\mu>|$ and its root of mean square $(<\mu^2>)^{1/2}$ for polar compounds listed in Table 2 are nearly identical, indicating that these quantities are well converged in the computer simulation. However, the difference for hydrocarbons and benzene is much larger than the estimated statistical uncertainty (Table 2). This observation implies that, although average dipole moments for methane, ethane, and benzene are zero in water, the instantaneous magnitude due to solvent polarization (see below) is not negligible and depends on the surrounding environment. The deviation is particularly large for benzene because it is much easier to polarize the π electron clouds than the σ electrons.

Results for the hydration of nucleotide bases and related compounds are summarized in Table 3. Here also we observe significant polarization effects for these molecules. Because both electron-withdrawing and electron-donating groups are present in these conjugated π systems, the polarization effect is somewhat greater than that of functional groups in amino acids. The polarization energy comprises about 15 to 20% of the electrostatic interaction between the bases and solvent. Cytosine has the largest

Table 2. Computed dipole moments μ (in debyes) in the gas phase and in water. The average standard deviation (±1σ) is about ±0.05 D for μ. The dipole moment for the anticonformation of acetic acid was computed with the 6-31G(d) basis set.

Compound	μ (gas)	μ (expt)	$<\mu>_{aq}$	$(<\mu^2>_{aq})^{1/2}$	μ_{ind}
CH_4	0	0	0.01	0.12	0.01
CH_3CH_3	0	0	0.03	0.17	0.03
C_6H_6	0	0	0.07	0.55	0.07
H_2O	1.86	1.85	2.15	2.15	0.29
CH_3OH	1.62	1.70	2.06	2.07	0.44
CH_3OCH_3	1.43	1.30	1.87	1.88	0.44
CH_3COCH_3	2.92	2.88	3.87	3.88	0.95
CH_3NH_2	1.49	1.31	1.69	1.70	0.20
CH_3CN	2.89	3.92	3.74	3.75	0.85
NMA	3.51	3.85	5.18	5.19	1.67
syn-CH_3CO_2H	1.89	1.74	2.21	2.23	0.32
anti-CH_3CO_2H	4.29	4.97	5.77	5.78	1.48
Imidazole	3.60	3.84	4.86	4.88	1.26

Table 3. Computed dipole moments (in debyes) and energies (in kilocalories per mole) for nucleotide bases. The simulations were carried out in a cubic box consisting of one solute molecule and 260 TIP3P water molecules. See also the legend of Table 1.

Compound	μ (gas)	μ (expt)	$<\mu>$	$E^{(1)}$	E_{pol}	E_{vdW}	E_{sx}
4-Pyridone	6.29	6.0	10.02	−26.5	−8.1	−7.9	−42.6
4-Aminopyrimidine	3.34	3.95	4.97	−11.7	−2.8	−8.8	−23.2
2-Aminopyrimidin-4-one	4.26	4.29	6.52	−24.1	−5.2	−9.7	−39.0
2,6-Diaminopyridine	0.01	1.46	0.30	−8.2	−1.9	−10.6	−20.6
4-Nitroaniline	7.64	6.2	10.77	−19.5	−3.9	−13.6	−37.0
Adenine	2.17	3.16	3.82	−13.9	−3.2	−10.6	−27.7
Cytosine	6.33	7.10	9.85	−33.8	−9.5	−8.4	−51.7
Guanine	6.18	6.76	8.47	−32.5	−6.5	−11.1	−50.1
Thymine	4.24	3.58	5.87	−23.8	−4.3	−9.8	−37.9
Uracil	4.28	3.86	5.85	−23.8	−3.9	−9.4	−37.1

polarization effect with 9.5 kcal/mol or 22% of the total electrostatic interaction energy. This result is in good accord with the finding of 30 to 50% polarization contribution to the total solvation energies by Honig and co-workers (*2*); however, the approximate solutions of the Poisson equation may lead to errors on the order of 50 to 100% (*2*). It is also interesting to compare the results for 4-pyridone (Table 3) with the AM1-SM2 prediction by Cramer and Truhlar (*30*). In that study, a dipole moment of 10.8 D was obtained with the partial charge on oxygen changing from −0.34 to −0.56 e in water. This result is in good accord with the calculated values of 10.0 D and −0.52 e by our Monte Carlo simulations.

To illustrate the polarization effects, an electron density difference (EDD) plot for cytosine at an instantaneous configuration in aqueous solution is shown in Fig. 4, and a stereoplot of the surrounding solvent structure near the first solvation layer is depicted in Fig. 5. Gains and losses in electron density indicated by the solid and dashed curves (Fig. 4) are revealed for the solute in water relative to the gas phase. Obviously, hydrogen bonding is a dominant factor in the solvent polarization effect (Figs. 4 and 5). The amino group in cytosine exhibited an "uneven" polarization effect with a larger depletion in electron density on the hydrogen (H) opposite to the Watson-Crick binding site (H′) (Fig. 4). Inspecting the solvent configuration shown in Fig. 5 indicates that a strong hydrogen bond between a water hydrogen and nitrogen (see also Fig. 1) creates electric and steric congestions, preventing another water molecule from forming a hydrogen bond with the amino hydrogen H′. Of course, Fig. 5 shows only one typical configuration of the 1.5 million sampled, although it is consistent with the computed average atomic charges from Mulliken population analysis, which yielded increases of 0.044 ± 0.003 e on H and 0.014 ± 0.002 e on H′. EDD can also be averaged in the Monte Carlo simulations, which may be compared with results from ab initio SCRF (self-consistent reaction field) models representing an average effect of the solvent (*31*).

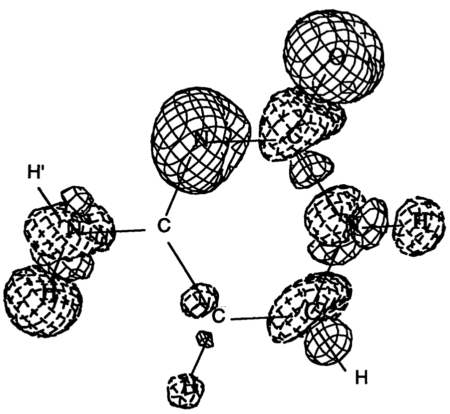

Fig. 4. Electron density difference plot for cytosine in water. Dotted contours represent regions where there is a depletion of electron density, and solid curves indicate areas where there is a gain in electron density, upon transferring the solute from the gas phase into aqueous solution. The surrounding solvent molecules are shown in Fig. 5.

Analysis of the Monte Carlo QM-MM simulations of organic molecules in aqueous solution revealed quantitative contributions of the polarization effects to the total electrostatic interaction energy between solute and solvent. That the polarization energy comprises about 10 to 20% of the total electrostatic interaction is significant and surprising, although this is in agreement with predictions by Honig and coworkers and by Cramer and Truhlar using continuum models (*2, 30*). Further, it is important to realize that effective potentials are predominantly utilized in current molecular dynamics and Monte Carlo simulations without explicitly incorporating the polarization effects (*3, 4*). Although excellent agreement between theoretical and experimental results can be obtained (*3, 4, 25*), it has been indicated that the accuracy perhaps can only be attained nonphysically (*2, 30*). Because quantum simulations of condensed-phase systems are not computationally practical in the near future (*32*), the hybrid AM1-TIP3P method, though precedented (*7*), provides an alternative, general approach for the study of the electronic effects in condensed-phase simulations. Of course, the AM1 theory used in the present study is an approximate, semiempirical method; however, it has wide application in biomolecular systems because of its tremendous computational efficiency and accuracy for many classes of reactions (*22*). The polarization energy decomposition method can shed new light on the nature of molecular interactions in solution. The accuracy of the method demonstrated here is encouraging, and the method should be useful for the parameterization of empirical polarizable intermolecular potentials.

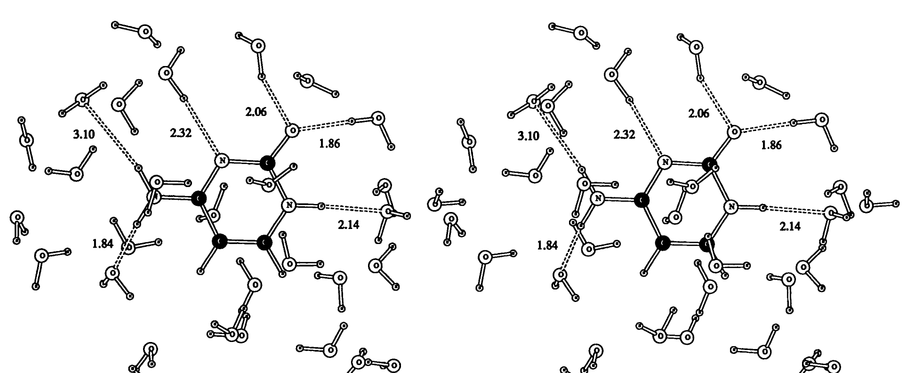

Fig. 5. Stereoplot of an instantaneous configuration from the Monte Carlo simulation of cytosine in water using the AM1-TIP3P model. For clarity, water molecules that are more than 4.5 Å from any solute atoms have been removed. The plot was made with the MindTool program written by J. Blake and J. Tirado-Rives.

REFERENCES AND NOTES

1. P. Barnes, J. L. Finney, J. D. Nicholas, J. E. Quinn, *Nature* **282**, 459 (1979); D. van Belle, I. Couplet, M. Prevost, S. J. Wodak, *J. Mol. Biol.* **198**, 721 (1987); L. X. Dang, J. E. Rice, J. Caldwell, P. A. Kollman, *J. Am. Chem. Soc.* **113**, 2481 (1991).
2. K. Sharp, A. Jean-Charles, B. Honig, *J. Phys. Chem.* **96**, 3822 (1992); A. Warshel and M. Levitt, *J. Mol. Biol.* **103**, 227 (1976).
3. M. Karplus and G. A. Petsko, *Nature* **347**, 631 (1990); W. F. van Gunsteren and H. J. C. Berendsen, *Angew, Chem. Int. Ed. Engl.* **29**, 992 (1990).
4. J. A. McCammon and S. C. Harvey, *Dynamics of Proteins and Nucleic Acids* (Cambridge Univ Press, Cambridge, 1987); M. P. Allen and D. J. Tildesley, *Computer Simulations of Liquids* (Oxford Univ. Press, London, 1987).
5. W. L. Jorgensen and J. Tirado-Rives, *J. Am. Chem. Soc.* **110**, 1657 (1988); J. Pranata, S. G. Wierschke, W. L. Jorgensen, *ibid.* **113**, 2810 (1991).
6. S. J. Weiner *et al.*, *ibid.* **106**, 765 (1984); B. R. Brooks *et al.*, *J. Comput. Chem.* **4**, 187 (1983).
7. M. J. Field, P. A. Bash, M. Karplus, *J. Comput. Chem.* **11**, 700 (1990), and references therein. This paper contains an extensive review of early works: I. S. Wang and M. Karplus, *J. Am. Chem. Soc.* **95**, 8160 (1973); A. Wahshel and M. Karplus, *ibid.* **94**, 5612 (1972).
8. J. H. McCreery, R. E Christoffersen, G. C. Hall, *J. Am. Chem. Soc.* **98**, 7191 (1976); B. T. Thole, and P. Th. van Duijnen, *Chem. Phys.* **71**, 211 (1982).
9. M. M. Karelson, A. R. Katritzky, M. Szafran, M. C. Zerner, *J. Org. Chem.* **54**, 6030 (1989).
10. V. Luzhkov and A. Warshel, *J. Comput. Chem.* **13**, 199 (1992); A. Warshel and S. Russel, *Q. Rev. Biophys.* **17**, 283 (1984); A. Warshel, *Computer Modeling of Chemical Reactions in Enzymes and Solutions* (Wiley, New York, 1991).
11. O. Tapia and B. Silvl, *J. Phys. Chem.* **84**, 2646 (1980); O. Tapia, F Colonna, J. G. Angyan, *J. Chim. Phys Phys Chim. Biol.* **87**, 875 (1990); S Miertus, E Scrocco, J. Tomasi, *Chem. Phys.* **55**, 117 (1981).
12. J. Gao, *J. Phys. Chem.* **96**, 537 (1992); ____ and J. J. Pavelites, *J. Am. Chem. Soc.* **114**, 1912 (1992)
13. J. D. Bernal and F. D. Fowler, *J. Chem. Phys.* **1**, 515 (1933).
14. S. J. Weiner, G. L. Seibel, P. A. Kollman, *Proc.*

Natl. Acad. Sci. U.S.A. **83**, 649 (1986); J.-K. Hwang, G. King, S. Greighton, A. Warshel, *J. Am. Chem. Soc.* **110**, 5297 (1988); B. Waszkowycz, I. H. Hillier, N. Gensmantel, D. W. Payling, *J. Chem. Soc. Perkin Trans. 2* **1991**, 225 (1991); P. A. Bash *et al.*, *Biochemistry* **30**, 5826 (1991).

15. P. A. Bash, M. J. Field, M. Karplus, *J. Am. Chem. Soc.* **109**, 8192 (1987).
16. F. Floris and J. Tomasi, *J. Comput. Chem.* **10**, 616 (1989). The Lennard-Jones term accounts for the solute-solvent dispersion interaction that was neglected by the off-diagonal elements in the density matrix. In the present study, the following parameters were adopted (σ in angstroms, ϵ in kilocalories per mole): C (3.50, 0.08); H (on C: 2.00, 0.01); H (on heteroatoms: 0.80, 0.10); O (sp^2: 2.95, 0.20); O (sp^3: 2.10, 0.15); O (water: 2.60, 0.15); N (2.50, 0.14); N (in NH and NH_2: 2.80, 0.15); N (in ammonium ions: 3.10, 0.16).
17. An effective potential was adopted for the solvent here. This is particularly advantageous in the present study over a polarizable potential such as the polarizable dipole model used by Warshel and co-workers (*10*) because the solute polarization properties, which are of the primary interest, can specifically be evaluated and decomposed. In addition, the TIP3P potential can also provide an excellent representation of the bulk structure and energy. An effective solvent potential as used here implies that the solvent polarization is already self-consistent, whereas the difference in the bulk and near the solute is negligible. Analogously, a uniform dielectric constant for the solvent has been widely used in continuum models including the work by Honig and co-workers (*2*). Remarkable agreement with experiment for ionic solvation has been obtained (*2*).
18. C. J. F. Bottcher, *Theory of Electric Polarization* (Elsevier, Amsterdam, 1973).
19. J. A. Pople and D. L. Beveridge, *Approximate Molecular Orbital Theory* (McGraw-Hill, New York, 1970); W. J. Hehre, L. Radom, P. v. R. Schleyer, J. A. Pople, *Ab Initio Molecular Orbital Theory* (Wiley, New York, 1986).
20. W. L. Jorgensen, J. Chandrasekhar, J. D. Madura, R. W. Impey, M. L. Klein, *J. Chem. Phys.* **79**, 926 (1983).
21. W. L. Jorgensen, *BOSS, Version 3.0* (Department of Chemistry, Yale University, New Haven, CT, 1991); J. Gao, *MCQUB* (Monte Carlo QM-MM at University at Buffalo, Department of Chemistry, State University of New York, Buffalo, 1992).
22. M. J. S. Dewar, E. G. Zoebisch, E. F. Healy, J. J. P. Stewart, *J. Am. Chem. Soc.* **107**, 3902 (1985); M. J. S. Dewar, E. F. Healy, A. J. Holder, Y. C. Yuan, *J. Comput. Chem.* **11**, 541 (1990); J. J. P. Stewart, *ibid.*, p. 543.
23. J. J. P. Stewart, *MOPAC*, Version 5 [Quantum Chemistry Program Exchange **6** (no. 391), 455 (1986)].
24. R. W. Zwanzig, *J. Chem. Phys.* **22**, 1420 (1954).
25. D. L. Beveridge and F. M. DiCapua, *Annu. Rev. Biophys. Biophys. Chem.* **18**, 431 (1989); W. L. Jorgensen, *Acc. Chem. Res.* **22**, 184 (1989); P. A. Kollman and K. M. Mertz, *ibid.* **23**, 246 (1990).
26. R. Wolfenden, L. Andersson, P. M. Cullis, C. C. B. Southgate, *Biochemistry* **20**, 849 (1981); A. Ben-Naim and Y. Marcus, *J. Chem. Phys.* **81**, 2016 (1984); R. G. Pearson, *J. Am. Chem. Soc.* **108**, 6109 (1986).
27. J. A. Piccirilli, T. Krauch, S. E. Moroney, S. A. Benner, *Nature* **343**, 33 (1990); M. Perutz, *Mechanisms of Cooperativity and Allosteric Regulation in Proteins* (Cambridge Univ. Press, Cambridge, 1990); J. Gao, K. Kuczera, B. Tidor, M. Karplus, *Science* **244**, 1069 (1989); T. J. Murray and S. C. Zimmerman, *J. Am. Chem. Soc.* **114**, 4010 (1992).
28. C. P. Smyth, *Dielectric Behavior and Structure: Dielectric Constant and Loss, Dipole Moment and Molecular Structure* (McGraw-Hill, New York, 1955).
29. J. G. Kirkwood, *J. Chem. Phys.* **2**, 351 (1934); L. Onsager, *J. Am. Chem. Soc.* **58**, 1486 (1936); W. C. Still, A. Tempczak, R. C. Hawley, T. Hendrickson, *ibid.* **112**, 6127 (1990).
30. C. J. Cramer and D. G. Truhlar, *Science* **256**, 213 (1992); *J. Am. Chem. Soc.* **113**, 8305 (1991); *ibid.*, p. 8552.
31. M. W. Wong, M. J. Frisch, K. B. Wiberg, *J. Am. Chem. Soc.* **113**, 4776 (1991).
32. D. Ceperley and B. Alder, *Science* **231**, 555 (1986); C. Zheng, C. F. Wong, J. A. McCammon, P. G. Wolynes, *Nature* **334**, 726 (1988).
33. We thank B. R. Brooks, M. J. Field, H. F. King, R. W. Pastor, and D. G. Truhlar for comments on this work. This work has been stimulated by conversations with M. Karplus who posed the question of the significance of quantitative polarization contributions to the total electrostatic energy. The Petroleum Research Fund, administered by the American Chemical Society, the NIH (Biomedical Research Support Grants), and the State University of New York (SUNY) at Buffalo provided support for this research. The calculations were done on a SUN SparcStation 2 and a Titan 3000 at SUNY at Buffalo.

3 June 1992; accepted 11 August 1992

Mercury Radar Imaging: Evidence for Polar Ice

Martin A. Slade,* Bryan J. Butler, Duane O. Muhleman

The first unambiguous full-disk radar mapping of Mercury at 3.5-centimeter wavelength, with the Goldstone 70-meter antenna transmitting and 26 antennas of the Very Large Array receiving, has provided evidence for the presence of polar ice. The radar experiments, conducted on 8 and 23 August 1991, were designed to image the half of Mercury not photographed by Mariner 10. The orbital geometry allowed viewing beyond the north pole of Mercury; a highly reflective region was clearly visible on the north pole during both experiments. This polar region has areas in which the circular polarization ratio (μ_c) was 1.0 to 1.4; values $<\sim 0.1$ are typical for terrestrial planets. Such high values of μ_c have hitherto been observed in radar observations only from icy regions of Mars and icy outer planet satellites.

Icy surfaces are common in the solar system, particularly on the moons of Jupiter and the rest of the outer planets. However, we were surprised to find that ice could exist on Mercury, the planet nearest the sun. Temperatures on Mercury reach as high as 700 K on the equator. Nevertheless, we interpret that a highly radar-reflective region observed on the north pole of Mercury in August 1991 is due to ices. The existence of the bright north polar feature was quickly confirmed at Arecibo, and a compact feature near the south pole was also discovered (*1*). We find that ices can be stable at the poles of Mercury over billions of years (*2*) owing to the temperature regimes (*3*) there. In this report, we present the observations that lead to the unexpected conclusion of ice on Mercury.

Observations of Mercury by ground-based or even space-based optical techniques are hampered by its close proximity to the sun (the greatest separation from the sun is about 28°). Spacecraft observations are difficult because of Mercury's depth in the sun's gravity well. Radar and radio methods (*4*, *5*) have played an important role in modern observations of Mercury because these techniques are relatively insensitive to solar constraints on observations. For example, Mercury's rotation was believed to be synchronously locked to the sun at an 88-day period (*6*) until continuous wave radar observations by Pettengill and Dyce (*7*) provided the first correct measurement of the period at 59 days. The topography of the equatorial regions of Mercury has been well studied with conventional delay-Doppler radar techniques (*5*, *8*). In visible light, the only images at useful resolutions were obtained by Mariner-10 in 1974–1975, which mapped roughly half of the planet (*9*). The geological interpretations of these images were summarized as "an extraordinary similarity to the surface of the moon" (*9*). However, in contrast with the moon, Mercury has a relatively strong magnetic field (*10*) and a surface gravity similar to that of Mars. Mercury's surface is left as the most poorly mapped of the terrestrial planets with completion of the radar mapping of the Venus surface by Magellan. Mercury has been characterized as an "end member" of the terrestrial planets by Chapman (*6*) because of its location, size, and density. Comparative planetology of the terrestrial planets is seriously compromised by the absence of a complete sample of Mercury.

To obtain additional data on the unmapped portion of Mercury's surface, we conducted radar observations on 8 August and again on 23 August 1991. Our system consisted of the National Aeronautics and Space Administration/Jet Propulsion Laboratory (NASA/JPL) Goldstone 70-m transmitter and the Very Large Array (VLA) at the National Radio Astronomy Observatory in Socorro, New Mexico, as the receiving instrument. A new technique in radar

---

M. A. Slade, Jet Propulsion Laboratory, California Institute of Technology, Pasadena, CA 91109–8099.
B. J. Butler and D. O. Muhleman, Division of Geological and Planetary Sciences, California Institute of Technology, Pasadena, CA 91125.

*To whom correspondence should be addressed.